ACS APPLIED MATERIALS & INTERFACES

Research Article

www.acsami.org

(001) $SrTiO_3$ | (001) MgO Interface and Oxygen-Vacancy Stability from First-Principles Calculations

Dilpuneet S. Aidhy,*[,†] Yanwen Zhang,[†,‡] and William J. Weber[†,‡]

[†]Materials Science and Technology Division, Oak Ridge National Laboratory, Oak Ridge, Tennessee 37831, United States

[‡]Materials Science and Engineering, University of Tennessee, Knoxville, Tennessee 37996, United States

ABSTRACT: In-depth understanding of interfacial atomistic structures is required to design heterointerfaces with controlled functionalities. Using density functional theory calculations, we investigate the interfacial structure of (001) $SrTiO_3$ | (001) MgO, and characterize the stable interface structure. Among the four types of possible interface structures, we show that the TiO_2-terminated $SrTiO_3$ containing electrostatically attractive Mg−O and Ti−O ion−ion interactions forms the most stable interface. We also show that oxygen vacancies can be preferentially stabilized across the interface via manipulating interfacial strain. We elucidate that oxygen vacancies are most stable in the tensile-strain material, and unstable in compressive strain material. This stability is explained from equation-of-state analysis using a single crystal, where the oxygen vacancy shows a larger volume than the oxygen ion, thus explaining its stability under tensile-strained conditions.

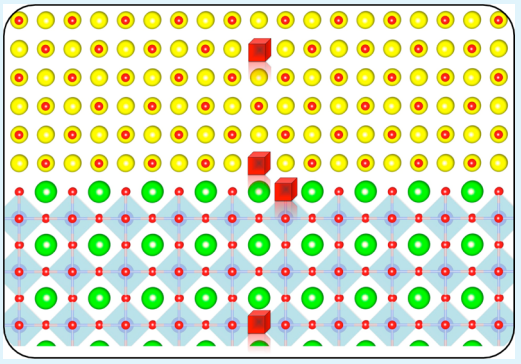

KEYWORDS: *Strain, heterointerfaces, MgO, $SrTiO_3$, oxygen vacancy, density functional theory*

1. INTRODUCTION

Over the past decade, heterointerfacing has emerged as one of the most interesting materials design parameters.[1−7] These interfaces, particularly for perovskite-based oxides, are functionalized by interfacial strain and show a variety of strikingly novel properties, and as a result, such heterointerface structures are exceedingly becoming key materials of technological interest.[3,5,7−10] For example, in the case of ion-transport, triggered by a study of the YSZ | $SrTiO_3$ interface,[6] increases in oxygen conductivity of several orders of magnitude have been achieved in ion-conducting interface systems.[11] The transition temperatures in superconducting $La_{2-x}Sr_xCuO_4$ | $SrTiO_3$,[12] ferromagnetic $LaCoO_3$ | $LaAlO_3$,[13] and ferroelectric $BaTiO_3$ | $DyScO_3$[14] interfaces have been significantly increased by interfacial engineering.[15] Similarly, multiferroicity and two-dimensional electron gas (2DEGs) heterostructures are other recent examples where materials' interfacing is being heavily exploited.[3,16] Heterointerfacing is also being actively pursued in designing materials for enhanced catalytic activity,[11] radiation tolerance,[17] and thermoelectric properties.[18] Meanwhile, understanding the interfacial atomistic structure remains one of the most important challenges to gain precise control over heterointerface design.[19−21]

$SrTiO_3$ | MgO is an interface of technological interest that has been studied extensively.[22−27] This interface was used to grow samaria-doped ceria thin films, i.e., SDC | STO | MgO to combine the chemical and thermal stability of the insulating MgO substrate with the structural properties of SDC | STO interface for oxygen conduction applications.[28] $BaTiO_3$ | $SrTiO_3$ multilayers grown on (001) MgO showed enhanced microwave dielectric properties with very low dielectric loss and high dielectric tenability.[29] The STO | MgO interface also serves as a model oxide interface to understand oxygen vacancy energetics, misfit dislocations, atomic intermixing, and other interfacial features. Until recently, understanding developed on the $SrTiO_3$ | MgO interface had suggested that interfacing between the two materials could only occur via a TiO_2-terminated $SrTiO_3$ surface, whereas SrO-terminated growth of MgO may not be possible.[24] This was attributed to the electrostatic atomistic repulsion, i.e., cation−cation repulsion between Sr and Mg in one case, or O−O repulsion in the other case during the layer-by-layer SrO-terminated $SrTiO_3$ | MgO stacking.[22] Similar observations were also made theoretically via density functional theory (DFT) calculations, and TiO_2-terminated $SrTiO_3$ | MgO was found to be the thermodynamically stable interface.[23] However, in contrast to this long-standing understanding, a recent study using scanning transmission electron microscopy (STEM)[20] has revealed that both SrO and TiO_2 terminated surfaces can form stable $SrTiO_3$ | MgO epitaxial thin-film interfaces, and that the surface terminations could alternate between SrO and TiO_2 in the presence of atomic steps along the interface. Keeping in view this new observation, we investigate the interface using DFT calculations, and characterize the stability of the four possible interface types.

Received: July 2, 2014
Accepted: August 19, 2014
Published: August 19, 2014

During oxide thin film growth, the formation of point defects, such as oxygen vacancies, is difficult to avoid. In addition, at various instances, these vacancies have been found to be beneficial to materials design as they induce novel interfacial electronic and ionic properties.[6,30] In view of the interfacial strain that is inherently present due to lattice mismatch, understanding the effect of strain on the concentration of oxygen vacancies could lead to preferential control of a stable vacancy concentration on either side of the interface. Such control on oxygen vacancy concentration would provide a new *"knob"* by which to tailor functionality in materials design. In this paper, we elucidate the (001) $SrTiO_3$ | (001) MgO interface, and based on those results, we predict the stability of neutral oxygen vacancies and provide a path to gain control over their precise location.

2. METHODOLOGY

We use the Vienna Ab Initio Simulation Package (VASP) for the DFT calculations.[31] In particular, the projector-augmented wave (PAW) method with plane waves up to the energy cutoff of 500 eV is used, and the exchange-correlation is evaluated by the generalized-gradient approximation (GGA) using the Perdew–Burke–Ernzerhof (PBE) function.[32] The reference electronic configurations are $2s^2p^4$, $3s^2$, $4s^24p^65s^2$, and $3d^34s^1$ for O, Mg, Sr, and Ti, respectively. All relaxations are done until the forces were smaller than 0.01 eV/Å. A *k*-point sampling of 2 × 2 × 1 is used for all interface structures. All calculations represent equilibrium structures. The bulk lattice parameters of MgO and $SrTiO_3$ obtained by full relaxation of 1 × 1 × 1 unit cells are 4.24 and 3.94 Å, respectively, which are within 2% of the experimentally reported values.

To provide a comparison with previous literature, the oxygen vacancy formation energy (ΔE^f) in bulk $SrTiO_3$ and MgO is calculated using the following expression:

$$\Delta E^f = E_v - E_p + \mu_O \quad (1)$$

Here, E_v is the system energy with a vacancy, E_p is the pure system energy, and μ_O is the oxygen chemical potential with reference to oxygen gas. The O_2 gas reference state is taken as the total energy for the ground state of a spin-polarized optimized oxygen molecule in the gas phase. We find that DFT literature values of ΔE^f for $SrTiO_3$ vary between 5.11 and 8.56 eV.[33−36] In addition, the formation energy is found to be dependent on the system size and concentration of oxygen vacancies.[36] From our calculations, we find ΔE^f to be 5.64 eV using a 3 × 3 × 3 supercell containing 135 atoms. Similarly, ΔE^f for MgO varies between 5.83 and 10.08 eV in the literature,[37,38] and our calculated value is 6.71 eV obtained from using a 3 × 3 × 3 supercell containing 216 atoms. While our ΔE^f values lie within the wide ranges in the literature, it is to be noted that, in this work, the vacancy stability across the interface structure is presented with reference to its location at the interface.

3. RESULTS

3.1. (001) $SrTiO_3$ | (001) MgO Interface. Based on the terminating plane of $SrTiO_3$, there are four possible cases that could arise while interfacing $SrTiO_3$ with MgO, as shown in Figure 1. Figure 1a,b shows SrO-terminated $SrTiO_3$; whereas Figure 1c,d shows TiO_2-terminated $SrTiO_3$, all interfaced with MgO. In the first case, labeled as type-a, there are Sr–Mg and O–Mg nearest-neighbor interactions; whereas in the second case (type-b), there are Sr–O and O–O nearest-neighbor interactions. In type-a, O–Mg is electrostatically attractive and Sr–Mg is repulsive, whereas in type-b, Sr–O is attractive and O–O is repulsive. In the TiO_2 terminated type-c and type-d cases, there are O–Mg and Ti–O interactions and O–O and Ti–Mg interactions, respectively. Among all these configurations, type-c is the only case that has no cation–cation or anion–anion repulsive interactions.

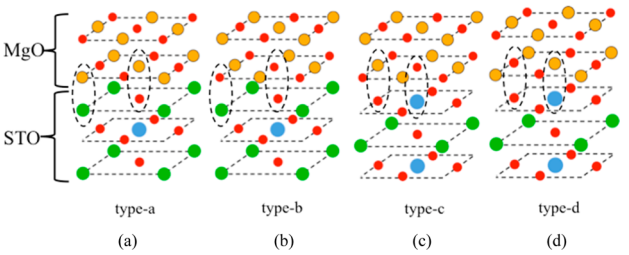

Figure 1. (001) $SrTiO_3$ | (001) MgO interfaces. (a) SrO-terminated with Sr–Mg and O–Mg interfacing labeled as type-a. (b) SrO-terminated with Sr–O and O–O interfacing (type-b). (c) TiO_2-terminated with O–Mg and Ti–O interfacing (type-c). (d) TiO_2-terminated with O–O and Ti–Mg interfacing (type-d). Color scheme: Sr in green, O in red, Ti in blue, and Mg in orange.

The interface formation energy, ΔE_{int}, is calculated using eq 2.

$$\Delta E_{int} = E_{int} - (E_{MgO} + E_{STO}) \quad (2)$$

Here, E_{int} is the total energy of the interface structure, and E_{MgO} and E_{STO} are the total energies of the individual MgO and STO supercells, respectively. In these calculations, we use equilibrated 1 × 1 × 6 rock salt unit cells for MgO and 1 × 1 × 12 perovskite unit cells for STO containing 48 and 60 atoms, respectively. In order to consider different surface terminations, a vacuum layer of 15 Å is added to both supercells. The vacuum layer creates TiO_2 and SrO terminations on two sides of the STO supercell. The terminations for MgO are same on both the sides. The two structures are then used to form the four interface structures in Figure 1. Furthermore, each interface structure is modeled so as to represent three different cases, i.e., (1) MgO film on $SrTiO_3$ interface, (2) $SrTiO_3$ film on MgO interface, and (3) a "multilayer" of $SrTiO_3$ and MgO. The first two cases are modeled by fixing the lattice parameters of the interface structure to those of $SrTiO_3$ and MgO in the $b \times c$ plane, respectively. The multilayer is modeled without applying such a constraint. For the calculation of interface energy from eq 2, E_{MgO} and E_{STO} are also calculated by fixing to the corresponding lattice parameters. For case (1), the lattice parameter of $SrTiO_3$ is used for calculation of both E_{MgO} and E_{STO}, whereas for case (2), MgO lattice parameter is used. For case (3), we first relax the interface structure, and then use the obtained supercell *b* and *c* directions to calculate E_{MgO} and E_{STO}.

A comparison of the interface formation energies for all four interface types, fixed to the corresponding lattice parameters, is shown in Figure 2. We find that the type-c interface is the most preferred interface among all four types. This stability is primarily due to the presence of the oppositely charged, electrostatically attractive interfacing ions, i.e., Ti–O and O–Mg. In addition, as pointed out earlier, this interface is the only type that does not contain similarly charged, repulsive direct ion–ion interactions. In contrast, the type-d interface, which is also a TiO_2 terminated interface, is the least stable interface. This instability originates from the two repulsive ion–ion interactions, i.e., between O–O and Ti–Mg. These DFT results are consistent with the previous experimental observations, where a TiO_2-terminated $SrTiO_3$ has been observed to be the most stable terminating surface interfacing with MgO. In addition, these results show that the interface is likely to

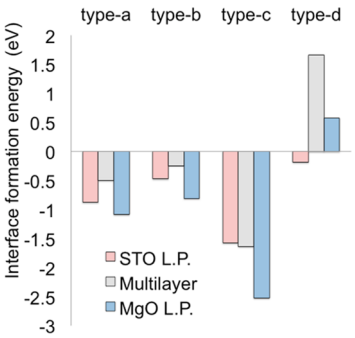

Figure 2. Interface formation energy comparison among four interface types. Type-a and type-b are SrO terminated, and type-c and type-d are TiO_2 terminated. For each type, the structure is strained to lattice parameters of STO, MgO, and multilayer. Type-c structure is the most stable interface structure.

contain Ti−O and O−Mg interactions, and Ti−Mg and O−O interfacing from type-d interface is unlikely to form.

The stability of SrO-terminated type-a and type-b structures lies in between the two TiO_2-interface structures. From the ion−ion interaction viewpoint, both structures contain one electrostatically attractive and one repulsive ion−ion interaction. Mg−O and Mg−Sr and O−Sr and O−O are the attractive and repulsive ion−ion interactions in type-a and type-b, respectively. Due to the presence of one repulsive interaction in both interfaces, the stability of SrO-terminated interfaces is less than the type-c TiO_2 terminated interface.

With reference to the recent observation where SrO-terminated interfaces have been observed in addition to TiO_2-terminated interfaces,[20] these DFT results indicate that the SrO-terminated interface is expected to be composed of type-a interface structure. While the DFT results show that TiO_2-terminated type-c would be the most dominant interface structure, accommodating defects such as misfit dislocations could be responsible for the stable SrO termination as captured in the TEM images.

3.2. Oxygen Vacancy Stability Across Interfaces. The effect of strain on kinetics of oxygen diffusion has recently been explored from atomistic modeling,[39,40] where it has been shown that tensile strain could be used to lower oxygen migration barriers. This understanding has provided a tailoring mechanism in the design of better oxygen conducting materials. From the vacancy stability viewpoint, it would be equally interesting to understand whether thermodynamics could be similarly altered such that one could preferably stabilize oxygen vacancies on either side of the interface. Here we perform the vacancy stability analysis across the interface, and predict that oxygen vacancies are likely to be stable in the tensile-strained material.

We explore the oxygen vacancy stability in type-c structure, which is the most preferable interface. An oxygen vacancy is placed at four different locations, i.e., inside $SrTiO_3$ (site A), at the TiO_2 terminated $SrTiO_3$ (site B), in MgO interfacing with $SrTiO_3$ (site C), and inside MgO (site D) as shown schematically in Figure 3a. The black squares and the dotted line represent the vacancy site and the interface, respectively. For each vacancy site, three calculations are carried out by fixing the lattice parameters in the $b \times c$ directions as above. In case 1 referred to as STO L.P. in Figure 3b, when the lattice parameters of $SrTiO_3$ are imposed, MgO undergoes compression from 4.24 to 3.93 Å in both $b \times c$ directions. In

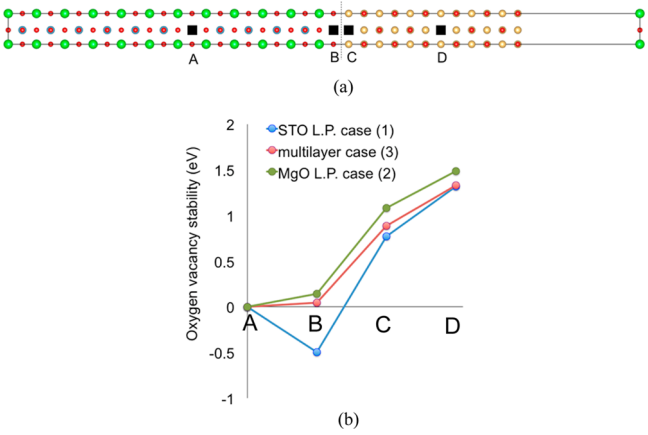

Figure 3. (a) Schematic representation of $SrTiO_3$−MgO interface structure showing four locations of oxygen vacancies (black squares). (b) Comparison of the oxygen vacancy stability at the four locations with reference to site A. Calculations are done for the three *cases* based on the strain on the structure. Site A is the most preferred vacancy location expect for case (1). Lines joining data points are shown as a guide to the eye..

case 2, MgO is maintained at its bulk lattice parameter, and STO undergoes tensile strain. In case 3, the interface relaxes to intermediate lattice parameters, i.e., to 4.03 Å, leading to expansion in $SrTiO_3$ and compression in MgO. The stability of the oxygen vacancy under these conditions is shown in Figure 3b with reference to site A. In all three cases, it is found that the oxygen vacancy is unstable in MgO and is stable in $SrTiO_3$. In addition, the vacancy is more stable inside $SrTiO_3$ at site A than at B, except for case 1. Furthermore, the energy difference between A and C (and D) increases by going from case 1 to case 3 to case 2 showing that as the tensile strain increases, the stability increases in favor of $SrTiO_3$. Therefore, these results indicate that a higher concentration of oxygen vacancies can be expected inside $SrTiO_3$ than MgO. In addition, these results show that for case 1 under imposed strain comparable to that of the lattice parameter of $SrTiO_3$, the vacancies can segregate near the interface, on the $SrTiO_3$ side.

This stability of oxygen vacancies under tensile stain can be understood from the equation-of-state analysis using a single crystal. Figure 4 shows E vs strain for $SrTiO_3$ for the bulk system (diamonds) and a system containing a vacancy

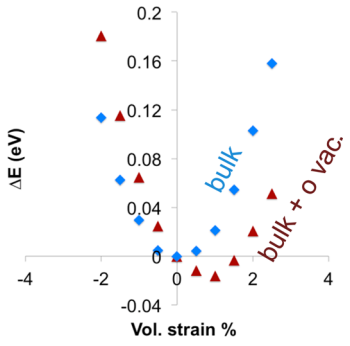

Figure 4. Energy vs strain profile for (a) bulk and (b) bulk containing an oxygen vacancy showing that oxygen vacancy occupies larger volume than oxygen ion, and is likely to be stable under tensile conditions.

(triangles). The energy profile is obtained using the following expression:

$$\Delta E = E_s - E_o \quad (3)$$

Here, ΔE is the change in the system energy under strain, E_s is the total energy of the strained system, and E_o is the total energy of the unstrained system. In comparison to the bulk system where the minimum energy occurs at 0 strain, the vacancy system instead shows the minimum under tensile strain, illustrating that oxygen vacancy occupies a larger volume compared to the oxygen ion. Such lattice expansion due to oxygen vacancy has been widely observed experimentally. Hence, in view of the strained interfaces, the oxygen vacancy is likely to be stable under tensile strain that provides a larger volume compared to compressive strain conditions.

To further explore the effect of tensile strain, the interface structure is strained beyond that of the case (2), i.e., even larger than the lattice parameter of MgO is applied in the $b \times c$ directions. Now, both $SrTiO_3$ and MgO are under tensile strain. The difference in the vacancy stability between sites A and D is plotted in Figure 5, which shows a 'V' curve where the stability

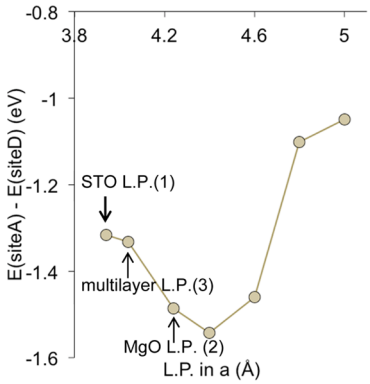

Figure 5. Oxygen vacancy stability difference between site A and site D. The stability shows a 'V' curve; there is a maximum stability until certain strain beyond which the stability starts to decrease.

difference between the two materials further increases. However, it starts to decrease beyond a certain strain. This behavior indicates that there is a limit to the stability that can be achieved via strain. Beyond that strain, not only does MgO start to undergo tensile strain thus providing stable conditions for the vacancy in MgO, but the parabolic nature of Figure 4 may also start to destabilize the vacancy in $SrTiO_3$. While such larger strains in Figure 5 may not be realistically possible, the simulations serve as a model to elucidate that strain can be used to modify vacancy stability/concentration. In addition, while larger strains do not completely flip the vacancy stability from $SrTiO_3$ to MgO, such a stability flip may not be implausible. This understanding could be particularly relevant to the multilayer structures, where choosing appropriate interfacing materials could preferentially alter the vacancy concentration.

CONCLUSION

We have carried out DFT calculations on the possible interface structures between $SrTiO_3$ and MgO to characterize their relative stability. We have found that, among the four possible interface structures, type-c TiO_2 terminated $SrTiO_3$ is the most stable interface that contains electrostatically attractive ion−ion interactions. The next possible interface structure is the SrO-terminated type-a structure. Keeping in view the recent SrO-terminated observation under experiments, we can attribute the stability to accommodating defects such as misfit dislocations that may play a key role in the interfacial relaxation. However, understanding of such defect-assisted stability requires future modeling efforts on interface structure consisting of misfit dislocations. We also find that the interfacing between similar charged ions, such as O−O or Mg−Ti in the type-d interface, during growth is less likely. Whether this ion−ion interaction is the reason behind the atomic interdiffusion across the interface observed under TEM needs to be further investigated from DFT calculations.

We also show that the control over the stability of oxygen vacancies can be gained via manipulating interfacial strain. We elucidate that oxygen vacancies are relatively more stable in the tensile-strained material, and are less stable in the compressive-strained material. Depending upon the amount of strain, the vacancies can also be preferentially stabilized at the interface. While to our knowledge there are no direct comparisons available, recent DFT calculations by Fronzi et al.[41] on bulk ZrO_2 and CeO_2 showed that tensile strain stabilized oxygen vacancies. It is worth noting that kinetics can alter the strain-affected thermodynamic stability/concentration. The stability of oxygen vacancy not only at the interface but away from it is dissimilar to the generally observed vacancy segregation that invariably occurs at grain boundaries. The grain boundary is a misorientation between crystals of the same material that have identical lattice parameters; in contrast, the interfaces have lattice mismatch from two different materials. This additional strain component across the interfaces leads to biased energetics. Hence, while grain boundaries are conventionally considered as sinks to vacancies, the sink strength of interfaces could depend on the interfacial strain, and the segregation of vacancies to interfaces may not be taken trivially. Apart from the lowering of oxygen migration barriers via tensile strain, stabilizing oxygen vacancies by interfacing would increase their concentration leading to further enhancement in oxygen conductivity. The concept of preferential vacancy localization by strain would be transferable to other heterointerfaces, and could provide a powerful control in materials design for a wide variety of interfacial materials for fast-ion conductors, superconductivity, ferromagnetic, and ferroelectric applications.

AUTHOR INFORMATION

Corresponding Author

*Phone: 865 241 2720. E-mail: aidhyds@ornl.gov.

Notes

The authors declare no competing financial interest.

ACKNOWLEDGMENTS

This research was supported by the U.S. Department of Energy, Basic Energy Sciences, Materials Science and Engineering Division. This research used resources of the National Energy Research Scientific Computing Center, which is supported by the Office of Science of the U.S. Department of Energy under Contract No. DE-AC02-05CH11231.

REFERENCES

(1) Sata, N.; Eberman, K.; Eberl, K.; Maier, J. Mesoscopic Fast Ion Conduction in Nanometer-Scale Planar Heterostructures. *Nature* **2000**, *408*, 946−949.

(2) Hwang, H. Y.; Iwasa, Y.; Kawasaki, M.; Keimer, B.; Nagaosa, N.; Tokura, Y. Emergent Phenomenon at Oxide Interfaces. *Nat. Mater.* **2012**, *11*, 103−113.
(3) Ohtomo, A.; Hwang, H. Y. A High-Mobility Electron Gas at the $LaAlO_3/SrTiO_3$ Heterointerface. *Nature* **2004**, *427*, 423−426.
(4) Rohrer, G. S.; Affatigato, M.; Backhaus, M.; Bordia, R. K.; Chan, H. M.; Curtarolo, S.; Demkov, A.; Eckstein, J. N.; Faber, K. T.; Garay, J. E.; Gogotsi, Y.; Huang, L.; Jones, L. E.; Kalinin, S. V.; Lad, R. J.; Levi, C. G.; Levy, J.; Maria, J.-P.; Mattos, L.; Navrotsky, A.; Orlovskaya, N.; Pantano, C.; Stebbins, J. F.; Sudarshan, T. S.; Tani, T.; Scott Weil, K.; Green, D. J. Challenges in Ceramic Science: A Report from the Workshop on Emerging Research Areas in Ceramic Science. *J. Am. Ceram. Soc.* **2012**, *95*, 3699−3712.
(5) Yu, P.; Chu, Y.-H.; Ramesh, R. Oxide Interfaces: Pathways to Novel Phenomena. *Mater. Today* **2012**, *15*, 320−327.
(6) Garcia-Barriocanal, J.; Rivera-Calzada, A.; Varela, M.; Sefrioui, Z.; Iborra, E.; Leon, C.; Pennycook, S. J.; Santamaria, J. Colossal Ionic Conductivity at Interfaces of Epitaxial ZrO_2: $Y_2O_3/SrTiO_3$ Heterostructures. *Science* **2008**, *321*, 676−680.
(7) Rivera-Calzada, A.; Diaz-Guillen, M. R.; Dura, O. J.; Sanchez-Santolino, G.; Pennycook, T. J.; Schmidt, R.; Bruno, F. Y.; Garcia-Barriocanal, J.; Sefrioui, Z.; Nemes, N. M.; Garcia-Hernandez, M.; Varela, M.; Leon, C.; Pantelides, S. T.; Pennycook, S. J.; Santamaria, J. Tailoring Interface Structure in Highly Strained YSZ/STO Heterostructures. *Adv. Mater.* **2011**, *23*, 5268−5274.
(8) Zubko, P.; Gariglio, S.; Gabay, M.; Ghosez, P.; Triscone, J.-M. Interface Physics in Complex Oxide Heterostructures. *Annu. Rev. Condens. Matter Phys.* **2011**, *2*, 141−165.
(9) Maier, J. Nanoionics: Ion Transport and Electrochemical Storage in Confined Systems. *Nat. Mater.* **2005**, *4*, 805−815.
(10) Granozio, F. M.; Koster, G.; Rijnders, G. Functional Oxide Interfaces. *MRS Bull.* **2013**, *38*, 1017−1023.
(11) Yildiz, B. Stretching" the Energy Landscape of Oxides—Effects on Electrocatalysis and Diffusion. *MRS Bull.* **2014**, *39*, 147−156.
(12) Bozovic, I.; Logvenov, G.; Belca, I.; Narimbetov, B.; Sveklo, I. Epitaxial Strain and Superconductivity in $La_{2-x}Sr_xCuO_4$ Thin Films. *Phys. Rev. Lett.* **2002**, *89*, 1070011−4.
(13) Fuchs, D.; Arac, E.; Pinta, C.; Schuppler, S.; Schneider, R.; v. Löhneysen, H. Tuning the Magnetic Properties of $LaCoO_3$ Thin Films by Epitaxial Strain. *Phys. Rev. B: Condens. Matter Mater. Phys.* **2008**, *77*, 0144341−8.
(14) Choi, K. J.; Biegalski, M.; Li, Y. L.; Sharan, A.; Schubert, J.; Uecker, R.; Reiche, P.; Chen, Y. B.; Pan, X. Q.; Gopalan, V.; Chen, L. Q.; Schlom, D. G.; Eom, C. B. Enhancement of Ferroelectricity in Strained $BaTiO_3$ Thin Films. *Science* **2004**, *306*, 1005−1009.
(15) Schlom, D. G.; Chen, L.-Q.; Fennie, C. J.; Gopalan, V.; Muller, D. A.; Pan, X.; Ramesh, R.; Uecker, R. Elastic Strain Engineering of Ferroic Oxides. *MRS Bull.* **2014**, *39*, 118−130.
(16) Ramesh, R. Complex Functional Oxide Heterostructures. *Curr. Sci.* **2013**, *105*, 1107−1114.
(17) Han, W.; Demkowicz, M. J.; Mara, N. A.; Fu, E.; Sinha, S.; Rollett, A. D.; Wang, Y.; Carpenter, J. S.; Beyerlein, I. J.; Misra, A. Design of Radiation Tolerant Materials Via Interface Engineering. *Adv. Mater.* **2013**, *25*, 6975−6979.
(18) Koumoto, K.; Wang, Y.; Zhang, R.; Kosuga, A.; Funahashi, R. Oxide Thermoelectric Materials: A Nanostructuring Approach. *Annu. Rev. Mater. Res.* **2010**, *40*, 363−394.
(19) Dyer, M. S.; Darling, G. R.; Claridge, J. B.; Rosseinsky, M. J. Chemical Bonding and Atomic Structure in Y_2O_3:ZrO_2-$SrTiO_3$ Layered Heterostructures. *Angew. Chem., Int. Ed.* **2012**, *51*, 3418−3422.
(20) Zhu, Y.; Song, C.; Minor, A. M.; Wang, H. Cs-Corrected Scanning Transmission Electron Microscopy Investigation of Dislocation Core Configurations at a $SrTiO_3$/MgO Heterogeneous Interface. *Microsc. Microanal.* **2013**, *19*, 706−715.
(21) Bi, Z.; Uberuaga, B. P.; Vernon, L. J.; Fu, E.; Wang, Y.; Li, N.; Wang, H.; Misra, A.; Jia, Q. X. Radiation Damage in Heteroepitaxial $BaTiO_3$ Thin Films on $SrTiO_3$ under Ne Ion Irradiation. *J. Appl. Phys.* **2013**, *113*, 0235131−8.
(22) McKee, R.; Walker, F.; Specht, E.; Jellison, G.; Boatner, L.; Harding, J. Interface Stability and the Growth of Optical Quality Perovskites on MgO. *Phys. Rev. Lett.* **1994**, *72*, 2741−2744.
(23) Cásek, P.; Bouette-Russo, S.; Finocchi, F.; Noguera, C. $SrTiO_3$(001) Thin Films on MgO(001): A Theoretical Study. *Phys. Rev. B: Condens. Matter Mater. Phys.* **2004**, *69*, 0854111−11.
(24) McMitchell, S. R. C.; Tse, Y. Y.; Bouyanfif, H.; Jackson, T. J.; Jones, I. P.; Lancaster, M. J. Two-Dimensional Growth of $Srtio_3$ Thin Films on (001) MgO Substrates Using Pulsed Laser Deposition and Reflection High Energy Electron Diffraction. *Appl. Phys. Lett.* **2009**, *95*, 1741021−3.
(25) Tse, Y. Y.; McMitchell, S. R. C.; Jackson, T. J.; Jones, I. P.; Genc, A. Line Defects, Planar Defects and Voids in $SrTiO_3$ Films Grown on MgO by Pulsed Laser and Pulsed Laser Interval Deposition. *Thin Solid Films* **2012**, *520*, 3440−3447.
(26) Li, H.; Roytburd, A. L.; Alpay, S. P.; Tran, T. D.; Salamanca-Riba, L.; Ramesh, R. Dependence of Dielectric Properties on Internal Stresses in Epitaxial Barium Strontium Titanate Thin Films. *Appl. Phys. Lett.* **2001**, *78*, 2354−2356.
(27) Meier, A. R.; Niu, F.; Wessels, B. W. Integration of $BaTiO_3$ on Si (001) Using MgO/STO Buffer Layers by Molecular Beam Epitaxy. *J. Cryst. Growth* **2006**, *294*, 401−406.
(28) Sanna, S.; Esposito, V.; Pergolesi, D.; Orsini, A.; Tebano, A.; Licoccia, S.; Balestrino, G.; Traversa, E. Fabrication and Electrochemical Properties of Epitaxial Samarium-Doped Ceria Films on $SrTiO_3$-Buffered MgO Substrates. *Adv. Funct. Mater.* **2009**, *19*, 1713−1719.
(29) Liu, M.; Ma, C.; Collins, G.; Liu, J.; Chen, C.; Alemayehu, A. D.; Subramanyam, G.; Ding, Y.; Chen, J.; Dai, C.; Lin, Y.; Cole, M. W. Ferroelectric $BaTiO_3/SrTiO_3$ Multilayered Thin Films for Room-Temperature Tunable Microwave Elements. *Nanoscale Res. Lett.* **2013**, *8*, 1−6.
(30) Borisevich, A. Y.; Lupini, A. R.; He, J.; Eliseev, E. A.; Morozovska, A. N.; Svechnikov, G. S.; Yu, P.; Chu, Y.-H.; Ramesh, R.; Pantelides, S. T.; Kalinin, S. V.; Pennycook, S. J. Interface Dipole between Two Metallic Oxides Caused by Localized Oxygen Vacancies. *Phys. Rev. B: Condens. Matter Mater. Phys.* **2012**, *86* (140102(R)), (1)−(6).
(31) Kresse, G.; Furthmuller, J. Efficiency of Ab-Initio Total Energy Calculations for Metels and Semicoonductors Using a Plane-Wave Basis Set. *Comput. Mater. Sci.* **1996**, *6*, 15−50.
(32) Perdew, J. P.; Burke, K.; Ernzerhof, M. Generalized Gradient Approximation Made Simple. *Phys. Rev. Lett.* **1996**, *77*, 3865−3868.
(33) D'Amico, N. R.; Cantele, G.; Ninno, D. First Principles Calculations of the Band Offset at $SrTiO_3$−TiO_2 Interfaces. *Appl. Phys. Lett.* **2012**, *101*, 1416061−4.
(34) Mitra, C.; Lin, C.; Robertson, J.; Demkov, A. A. Electronic Structure of Oxygen Vacancies in $SrTiO_3$ and $LaAlO_3$. *Phys. Rev. B: Condens. Matter Mater. Phys.* **2012**, *86*, 1551051−8.
(35) El-Mellouhi, F.; Brothers, E. N.; Lucero, M. J.; Scuseria, G. E. Neutral Defects in $SrTiO_3$ Studied with Screened Hybrid Density Functional Theory. *J. Phys.: Condens. Matter* **2013**, *25*, 1355011−8.
(36) Carrasco, J.; Illas, F.; Lopez, N.; Kotomin, E.; Zhukovskii, Y.; Evarestov, R.; Mastrikov, Y.; Piskunov, S.; Maier, J. First-Principles Calculations of the Atomic and Electronic Structure of F Centers in the Bulk and on the (001) Surface of $SrTiO_3$. *Phys. Rev. B: Condens. Matter Mater. Phys.* **2006**, *73*, 0641061−11.
(37) Tanaka, I.; Oba, F.; Tatsumi, K.; Kunisu, M.; Nakano, M.; Adachi, H. Theoretical Formation Energy of Oxygen-Vacancies in Oxides. *Mater. Trans.* **2003**, *43*, 1426−1429.
(38) Carrasco, J.; Lopez, N.; Illas, F. First Principles Analysis of the Stability and Diffusion of Oxygen Vacancies in Metal Oxides. *Phys. Rev. Lett.* **2004**, *93*, 2255021−4.
(39) De Souza, R. A.; Ramadan, A.; Hörner, S. Modifying the Barriers for Oxygen-Vacancy Migration in Fluorite-Structured CeO_2 Electrolytes through Strain: A Computer Simulation Study. *Energy Environ. Sci.* **2012**, *5*, 5445−5453.

(40) Rushton, M. J. D.; Chroneos, A.; Skinner, S. J.; Kilner, J. A.; Grimes, R. W. Effect of Strain on the Oxygen Diffusion in Yttria and Gadolinia Co-Doped Ceria. *Solid State Ionics* **2013**, *230*, 37−42.
(41) Fronzi, M.; Cereda, S.; Tateyama, Y.; De Vita, A.; Traversa, E. Ab Initio Investigation of Defect Formation at ZrO_2-CeO_2 Interfaces. *Phys. Rev. B: Condens. Matter Mater. Phys.* **2012**, *86*, 0854071−5.